Evaluating Yangtze River Delta Urban Agglomeration flood risk using hybrid method of AutoML and AHP

Yu Gao [1,2], Haipeng Lu [1,2], Yaru Zhang[1,2], Hengxu Jin[1,2], ~~Suai~~Shuai Wu[3], Yixuan Gao[1,2], Shuliang Zhang[1,2*]

1 Key Laboratory of VGE of Ministry of Education, Nanjing Normal University, Nanjing 210023, China

2 Jiangsu Center for Collaborative Innovation in Geographical Information Resource Development and Application, Nanjing 210023, China

3 Lianyungang Real Estate Registry, Lianyungang 222006, China

Correspondence to: Shuliang Zhang (zhangshuliang@njnu.edu.cn)

Abstract. With rapid urbanization, the scientific assessment of disaster risk caused by flooding events has become an essential task for disaster prevention and mitigation. However, adaptively selecting optimal machine learning (ML) models for flood risk assessment and further conducting spatial and temporal analyses of flood risk characteristics in urban agglomerations ~~remains~~remain challenging. This study, establishes a “H–E–V–R” risk assessment index system that integrates hazard, exposure, vulnerability, and resilience based on the factors influencing flood risk in the Yangtze River Delta Urban Agglomeration (YRDUA). Utilizing Automated Machine Learning (AutoML) and the Analytic Hierarchy Process (AHP), a comprehensive flood risk assessment model is constructed. Results indicate that, among those of different assessment models, the accuracy, precision, F1-score, and kappa coefficient of the Categorical Boosting (CatBoost) model for flooded point identification are the highest. Among the flood hazard factors, elevation ranks highest in importance, with a contribution rate of up to 68.55%. The spatial distribution of flood risk in the study area from 1990 to 2020 is heterogeneous, with an overall increasing risk trend. This study is of great significance for advancing disaster prevention, mitigation, and sustainable development in the YRDUA.

1 Introduction

Under global climate change and accelerated urbanization, China has been experiencing pervasive flooding ever more frequently (Tang et al., 2024). Floods threaten people's lives, hinder social development and cause huge economic losses in China (Anon, 2021; Echendu, 2020; Milanesi et al., 2015). Flood formation has been exacerbated by climate change and urbanization, leading to increased frequency, extent, and intensity of urban flooding, and impacting urban flood risk~~.~~ (Mahmoud and Gan, 2018; Khadka et al., 2023; Scott et al., 2023; Seemuangngam and Lin, 2024). Modern human society is faced with the possibility of serious flood hazards and associated challenges, and in addition to post-disaster emergency management, the scientific assessment of disaster risks arising from flood events has gradually become a crucial aspect in preventing and mitigating disasters.

Formatted

Currently, most research in the field of flooding focuses on the flood risks of individual cities~~.~~ ~~(Wang et al., 2021, 2023c; Guan et al., 2024)~~(Wang et al., 2021, 2023b; Guan et al., 2024). However, in recent years, the frequency and intensity of urban flooding in China have increased dramatically, and individual cities are no longer able to independently mitigate the risks arising from floods. Studies indicate that China's flood risk management needs to be transformed from the scale of isolated individual cities to the scale of urban agglomerations, conducted in a regionally coordinated manner ~~(Morales-Torres et al., 2016; Wang et al., 2023b).~~(Morales-Torres et al., 2016; Wang et al., 2023a). City clusters, constituting the spatial organizational structure of cities that have reached an advanced stage of development, have become key areas for regional disaster management and sustainable development. Due to the unique geographical location and climate conditions of the YRDUA, as well as the impact of urbanization over the past 30 years, the frequency and intensity of flood disasters have been increasing, posing a serious threat to the sustainable development of cities. Therefore, implementing relevant emergency management strategies for flood risks is urgently needed. Furthermore, the region comprises multiple cities, among which distinct resource interactions, such as population mobility and risk transfer, exist (Lu et al., 2022). Thus, it is essential to assess both the overall flood risk characteristics and changes in the urban agglomeration, as well as the spatial correlations of flood risks between cities, explore the mutual influences and interaction mechanisms among regional disaster risks, and provide a scientific basis for sustainable development within the urban agglomeration (Xu et al., 2024).

Statistical analyses of historical disaster statistics (Lang et al., 2004), indicator systems methods (Wang et al., 2018), scenario simulations methods (Yang et al., 2018), and data-driven methods (Abu-Salih et al., 2023), are the primary flood risk assessment method currently. With the development of artificial intelligence technology, data-driven methods, such as machine learning, deep learning, and artificial neural networks, have emerged, providing new opportunities for improving traditional flood risk assessment methods (Liu Jiafu and Zhang Bai, 2015). ~~As ML~~Through continuous improvement and development of machine learning algorithms~~ continue to develop and improve, integrated~~, ensemble methods ~~address~~have effectively addressed the limitations of ~~general ML~~traditional machine learning models~~ have emerged~~ (Kazienko et al., 2015). Various integrated ML methods have been utilized in hydrology, with the Boost algorithm being extensively applied for flood prediction and assessment (Shafizadeh-Moghadam et al., 2018; Mirzaei et al., 2021; Yan et al., 2024). However, these integrated

Formatted

Formatted

models lack preprocessing and feature selection capabilities, and their application effects vary considerably across different regions. To fully mine data and discover more effective features, experts have proposed other solutions, namely hybrid models such as ANFIS, LSTM-ALO, and LSSVM-GSA (Nayak et al., 2004; Yuan et al., 2018; Adnan et al., 2017). These methods have achieved good performances for given hydrological time series, focusing more on data preprocessing and feature selection. Although research on data-driven urban flood risk assessment methods has increased, certain limitations remain. For example, the physical importance of urban hydrological processes is often ignored in the model assessment process, interpretation of the assessment results is weak, and quantifying the boundaries and scales is challenging ~~(Abu-Salih et al., 2023; Guo et al., 2022)~~(Abu-Salih et al., 2023; Guo et al., 2022).

Furthermore, attempting to combine the data processing and feature selection capabilities of hybrid models with those of integrated models remains challenging (Li et al., 2017). Existing algorithms cannot perform well for all learning problems; thus, each ML component, such as feature engineering, model selection, and algorithm selection, must be carefully configured (Li et al., 2017; Raschka, 2020). Hence, ML applications require the participation of many experts, leading to disproportionate costs for ML development and improvement (Wagenaar et al., 2020; Sarro et al., 2022; Rashidi Shikhteymour et al., 2023). ~~Additionally, ML is not be fully automated, and its application effect improves empirically~~The effectiveness of machine learning "automatically improves with experience," and a key challenge in the research is how to integrate the data processing capabilities and feature selection strengths of hybrid models with ensemble models (Jordan and Mitchell, 2015; Nagarajah and Poravi, 2019). AutoML is an innovative ML framework designed for training ML models and addressing various problems~~.~~ (He et al., 2021; Consuegra-Ayala et al., 2022). However, AutoML has not been widely applied in the fields of hydrology and disaster risk management, and research has mainly focused on optimizing the integrated model to achieve better performance (Özdemir et al., 2023). Continuous research has highlighted the potential role of AutoML in flood risk detection and assessment (Guo et al., 2022; Vincent et al., 2023; Munim et al., 2024). Guo et al. (2022) compared AutoML with three single ML algorithms (CatBoost, XGBoost, and BPDNN) and concluded that AutoML performed better in building rapid warning and comprehensive analysis models for urban waterlogging. The model based on AutoML can be applied to areas without water level monitoring and achieve accurate predictions and rapid warnings of waterlogging depth (Guo et al., 2022; Yan et al., 2024). Abu-Salih et al. (2023) proposed a data-driven flood risk area detection model that combined the integrated model with the AutoML tool and successfully solved the problems of data balance and strategy modeling, while reducing the complexity of flood risk area prediction. Previous studies have provided a theoretical basis and scientific reference for the application of AutoML methods to flood risk assessment. However, the use of AutoML for research purposes is a complex issue, and many new opportunities and challenges remain regarding its specific applications.

Although AutoML can objectively and efficiently calculate flood risk, it lacks comprehensiveness and judgment. Therefore, when evaluating the indicators of various dimensions of flood risk, quantifying the impacts of different levels of each indicator on flood risk is impossible, and determining the indicator weight is challenging. Therefore, to determine the indicator weight, using relevant statistical methods is necessary. Multicriteria decision analysis (MCDA) is a useful tool for considering complex decision-making problems in flood risk management (Fernández and Lutz, 2010). The analytic hierarchy process (AHP) is one of the most popular MCDA techniques (Donegan et al., 1992). This technique emphasizes the importance of the subjective judgment of decision makers and the consistency of pairwise comparisons of standards in the decision-making process (Saaty, 1980). Recent studies have focused on integrated frameworks of ML models and MCDA technology for flood hazard assessment (Kanani-Sadat et al., 2019; Khosravi et al., 2019; Gudiyangada Nachappa et al., 2020; Mia et al., 2023). However, research focusing on using an integrated framework of AutoML and AHP techniques is still limited.

This study constructs a flood risk assessment model based on AutoML and AHP by examining the factors influencing flood risk in the YRDUA. Based on the proposed flood risk assessment model, the risk, exposure, vulnerability, and resilience as well as their corresponding weights of flooding in the YRDUA are calculated, and the regional flood risk level zoning map is obtained. ~~Comparative~~The comparative analysis of ~~the~~ superimposed flooded points data ~~reveals that~~shows a strong alignment between the distribution of flooded points in the study area ~~is basically consistent with the distribution of~~ and the high ~~and~~to medium-~~to-~~high risk areas ~~of flooding. The proportion of quantifying the distribution is 87.45%, indicating that the~~, highlighting the reliability and applicability of the proposed model ~~in~~. The remainder of this paper ~~performs well and has high credibility for flood risk assessment. The analysis of spatial~~is structured as follows: Section 2 describes the study area, data sources, and ~~temporal patterns of flood risk change over~~methodology; Section 3 presents the ~~past 30 years provides scientific basis~~results and

~~theoretical support for disaster prevention~~analysis; Section 4 discusses the findings and ~~mitigation in the YRDUA~~their implications; and Section 5 concludes the study with key insights and recommendations.

2 Materials and methods

In this section, the study area is briefly introduced (Section 2.1), and each individual component of the study is further discussed along with the basic geographic information, meteorology, social statistics, historical disaster data, and other fields involved in the study of urban agglomeration flood disasters and their risks (Section 2.2). The framework of the flood risk assessment model is shown in **Figure 1**. The factors influencing flood risk in the YRDUA are explored, and a flood risk assessment index system is established (Section 2.3). The optimal model in AutoML is selected to calculate the importance of flood hazard and hazard characteristic factors (Section 2.4), and the model is combined with AHP to determine the weight of each risk indicator (Section 2.5). Ultimately, a flood risk assessment model based on AutoML and AHP is constructed.

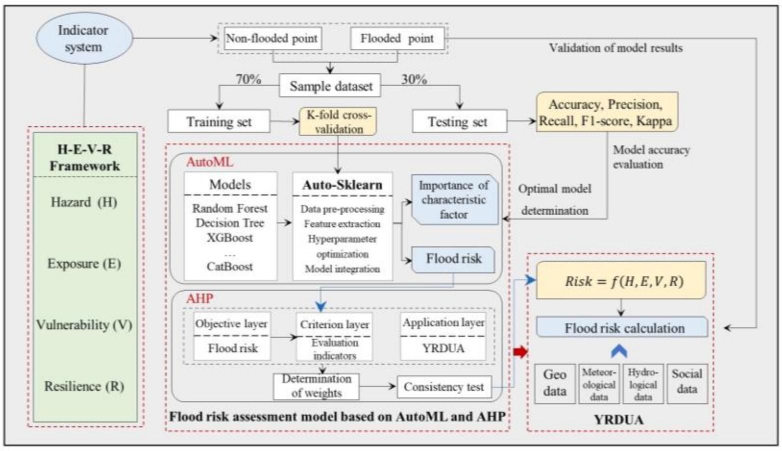

Figure 1: Flood risk assessment modeling framework.

2.1 Study area

The Yangtze River Delta Urban Agglomeration, located in the eastern coastal region of China (27° 04′–34° 49′ N; 115° 75′–122° 95′ E), includes 27 cities: 8 in Anhui Province, 9 in Jiangsu Province, 9 in Zhejiang Province, and Shanghai (**Figure 2**~~)~~) (Yang et al., 2024). Influenced by the East Asian summer monsoon, the study area features low-lying plains in the northern region and higher hilly terrain in the southern region, along with numerous waterways (Ding et al., 2021). With the recent accelerated climate change and urbanization, extreme precipitation events in the Yangtze River Delta (YRD) have been occurring ever more frequently, and the temporal and spatial distribution differences in precipitation have increased. Additionally, the increase in impervious surfaces, narrow plains rivers, and poor drainage may result in more frequent and widespread urban flooding and waterlogging disasters (Wan et al., 2013). This region is economically developed and densely populated , making it the largest urban agglomeration in Asia (Sun et al., 2023). In 2008, the Gross Domestic Product (GDP) of the YRD accounted for 17.5% of the GDP of the entire country, i.e., 4.3 trillion yuan, and the per capita GDP was 44,468 yuan, i.e., twice the national average level. The population has reached 97.2 million, i.e., 7.3% of China's total population, and the region's average population density is 877 persons/km^2, i.e., approximately twice the national average (Gu et al., 2011). Therefore, the potential risks of flood and waterlogging disasters are substantial.

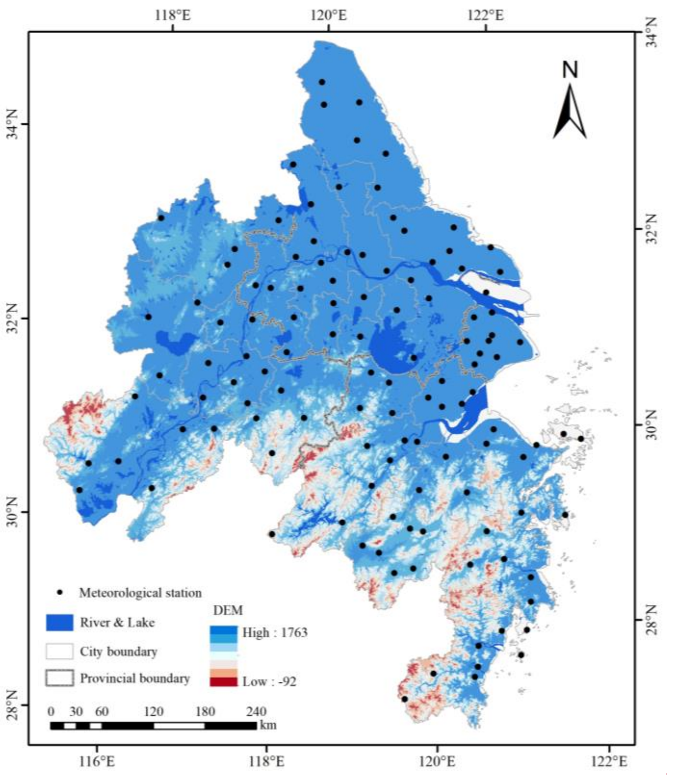

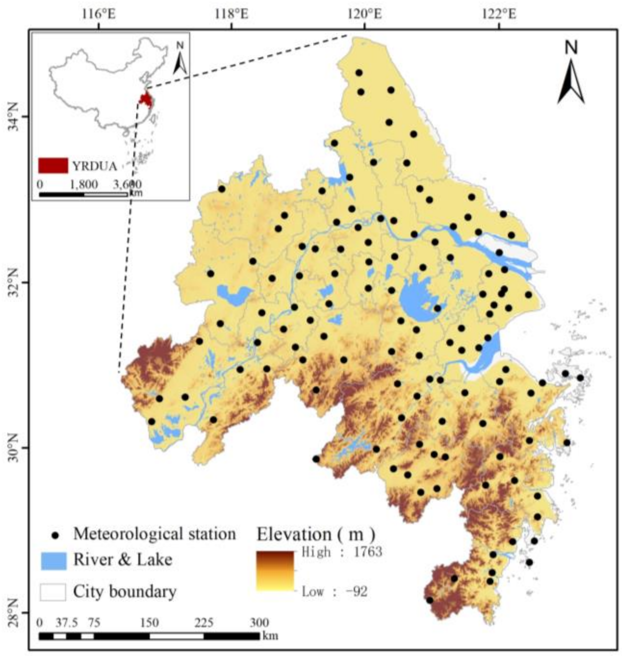

Figure 2: ~~Study area.~~**The schematic map of the YRDUA.**

2.2 Data sources and processing

2.2.1 Data sources

The study of flood disasters and their associated risks in urban agglomerations involves complex natural and ~~social~~socio-economic factors. Therefore, we collected and preprocessed data from multiple fields, such as basic geography, meteorology, social statistics, and historical disasters. **Table 1** lists the data types and resolutions collected for the research area.

Table 1: ~~**Data sources**~~**Description of the Datasets Used for Flood Risk Assessment, Their Characteristics, and Data Sources**.

Category~~Dataset~~	~~Data name~~Details	~~Spatial resolution~~Resolution	Data ~~source~~Source
Basic ~~geographic information~~	~~Basic geographic information data~~Administrative boundaries and river network density data.	~~Vector data~~30m	-Resources and Environmental Science and Data Center, ~~Chinese~~

Formatted: Font: (Default) +Headings (等线 Light), 10 pt, Not Bold,

Formatted: Heading 3,my标题3,章节三级标题

Formatted Table

Formatted: English (United States)

Formatted: English (United States)

Formatted: English (United States)

Formatted: Widow/Orphan control

Formatted: English (United States)

Formatted: Justified

Formatted: Justified, Widow/Orphan control

Merged Cells

Merged Cells

~~data~~Geographic Information Data			~~Academy of Sciences~~CAS (https://www.resdc.cn~~/)~~/) . -USGS (https://earthexplorer.usgs.gov/). -Wuhan University CLCD dataset (https://zenodo.org/records/8176941). - National Ecosystem Science Data Center (nesdc.org.cn).
	~~Digital elevation model~~	~~30 m~~	~~The U.S. geological survey (https://earthexplorer.usgs.gov/)~~
	~~River network density data~~Digital Elevation Model (DEM) based on SRTM1 (30m), mosaicked and clipped to the study area (27 core cities).	~~Vector data~~	~~Resources and Environmental Science and Data Center, Chinese Academy of Sciences (https://www.resdc.cn/)~~
	~~Land use data~~Land use data from CLCD (30m), includes 7 types: farmland, forest, shrubland, grassland, water, bare land, and impervious surfaces.	~~30 m~~	~~Wuhan University CLCD dataset (https://zenodo.org/records/8176941)~~
	~~Normalized difference vegetation index data~~	~~30 m~~	~~National Science and Technology Infrastructure - National Ecosystem science Data Center (http://www.nesdc.org.cn)~~
	~~Building data~~NDVI data (2000–2020) calculated using the GEE platform.	~~Vector data~~	~~OpenStreetMap (https://openstreetmap.maps.arcgis.com/)~~
Meteorological ~~data~~Data	~~Precipitation data~~Hourly precipitation data from 120 meteorological stations. Data preprocessed for outlier removal and missing value handling.	~~Site~~Station data	National Meteorological Information Center, China Meteorological Administration
Social ~~statistics~~Statistics	~~Population data~~Population, unemployment, GDP, and healthcare statistics at the prefecture level.	Prefecture-level	Provincial and municipal statistical yearbooks and bulletins
	~~Gross domestic product~~Urbanization rate calculated using urban population proportion.	~~Prefecture-level~~	~~Provincial and municipal statistical yearbooks and bulletins~~

Formatted: Justified
Merged Cells
Formatted: Justified, Widow/Orphan control
Formatted: Justified
Merged Cells
Formatted: Justified, Widow/Orphan control
Formatted: Justified
Merged Cells
Formatted: Justified, Widow/Orphan control
Merged Cells
Formatted: Widow/Orphan control
Formatted: English (United States)
Formatted: English (United States)
Formatted: English (United States)
Formatted: Justified, Widow/Orphan control
Formatted: Justified, Widow/Orphan control
Formatted: Widow/Orphan control
Formatted: English (United States)
Formatted: English (United States)
Formatted: English (United States)
Formatted: Justified, Widow/Orphan control
Merged Cells
Formatted: Justified
Merged Cells
Formatted: Justified
Formatted: Justified, Widow/Orphan control
Formatted: Justified

	~~Unemployment figures~~GDP density and per capita GDP derived from total GDP and land area/population.	~~Prefecture-level~~	~~Provincial and municipal statistical yearbooks and bulletins~~
	~~Health care statistics~~	~~Prefecture level~~	~~Provincial and municipal statistical yearbooks and bulletins~~
Historical ~~disaster data~~Disaster Data	~~Historical flooding data~~Flood inundation data from the MODIS-based Global Flood Database (2000–2018), processed to focus on the YRDUA region. To ensure comprehensive selection of inundation points, the inundated areas within the time frame were overlaid to produce a historical flood map.	~~250 m~~250m	Global Flood Database (https://www.emdat.be/)
	~~Historical flood hazard data~~	~~The statistics~~	~~EM-DAT database (https://www.emdat.be/)~~

2.2.2 Data standardization and preprocessing

Due to variations in data sources and formats, the collected flood disaster risk data exhibit differences in spatial resolution, dimensions, and magnitude. To ensure consistency and comparability, standardization of both spatial scale and numerical range was performed before using these datasets as flood risk indicators.

Unification of spatial scale means aligning data within the same coordinate range and resolution. The research data is standardized through projection transformation, converting all datasets into the same geographic and projected coordinate systems. The Kriging interpolation method is used to spatially process all discrete data. Finally, if the spatial data has different resolutions, resampling is performed to standardize all data to the same resolution, which in this study is unified to 30m×30m.

Normalization of the numerical range can be achieved using a normalization process. Through a linear transformation, the values of the data are mapped to the range [0, 1], thus eliminating the influence of differing dimensions among the data indicators. In this study, the Min-Max Normalization method is used for normalization, and the formula is given by Eq. (1) :

$$x' = \frac{x-\min(x)}{\max(x)-\min(x)}, \qquad (1)$$

Formatted: Justified, Widow/Orphan control
Formatted: Widow/Orphan control
Formatted: English (United States)
Formatted: English (United States)
Formatted: English (United States)
Split Cells
Formatted: Justified, Widow/Orphan control
Formatted Table
Formatted: Widow/Orphan control
Formatted: English (United States)
Formatted: Justified, Widow/Orphan control
Formatted: English (United States)
Formatted: Font: Bold, English (United States)
Formatted: English (United States)
Split Cells

2.3 Extraction of historical flood inundation points

The historical flood inundation map of the study area is shown in **Figure 3** (a). The flood inventory map used in this study was created based on inundation data from the Global Flood Database and the EM-DAT flood disaster database, and further verified through satellite imagery, Google Earth, and existing historical flood records. The actual flooded areas were delineated from flood traces in the inundation dataset and image interpretation. During the study period, 278 flooded points were randomly selected within the inundation data range. The location of each point serves as the foundation for subsequent statistical analysis of flood events, with the spatial distribution shown in **Figure 3** (b).

To calculate flood hazard, it is necessary to select training samples. The task of identifying flooded and non-flooded points using AutoML is essentially a binary classification problem, which requires a balanced number of samples. An imbalanced ratio of positive and negative samples can result in unreliable classification outcomes. Previous studies (Pham et al., 2021; Bostan et al., 2012) have shown that the best classification performance is achieved when the ratio of flooded to non-flooded points is 1:1. Therefore, after selecting the flooded points, 278 non-flooded points were randomly sampled to ensure a balanced 1:1 ratio, excluding high-altitude areas, based on the region's actual characteristics. Finally, the flooded and non-flooded points were used as sample data and divided into a 7:3 ratio (70% for training and 30% for testing) for model training.

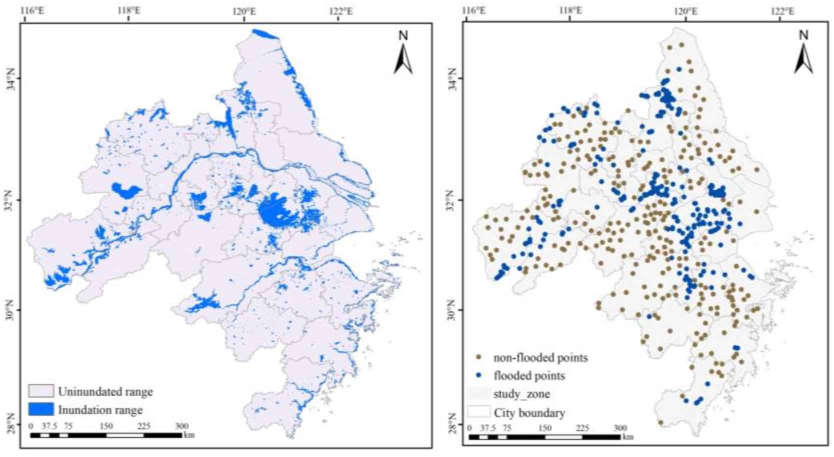

Figure 3: (a) Flood inundation map of the study area. (b) Spatial Distribution of Flooded and Non-Flooded Points in the YRDUA.

2.4 Establishment of ~~an~~a flood risk assessment indicator system

Although risk is a universal concept, it has no universal definition (Aven, 2016; Mishra and Sinha, 2020). Based on the hazard–exposure–vulnerability (H–E–V) disaster risk framework, we considered the particularity of flood risk research at the urban agglomeration scale, incorporated resilience indicators into the existing framework, and constructed a four-dimensional flood risk assessment framework of hazard–exposure–vulnerability–resilience (H–E–V–R) that can assess regional flood risks more comprehensively and systematically. The conceptual description of flood risk in this study can be expressed in the Eq. ~~(1)~~(2):

$$\cancel{Risk = f(H,E,V,R) = \sum_{i=1}^{a}\omega_H H_i + \sum_{i=1}^{b}\omega_E E_i + \sum_{i=1}^{c}\omega_V V_i + \sum_{i=1}^{d}\omega_R R_i, \quad (1)}$$

$$Risk = f(H,E,V,R) = \sum_{i=1}^{a}\omega_H H_i + \sum_{i=1}^{b}\omega_E E_i + \sum_{i=1}^{c}\omega_V V_i + \sum_{i=1}^{d}\omega_R R_i \quad (2)$$

where H, E, V, and R represent the danger of, exposure to, vulnerability to, and resilience in response to floods, respectively; ω_H, ω_E, ω_V, and ω_R are the weights of danger, exposure, vulnerability, and resilience, respectively; H_i, E_i, V_i, and R_i are the values of items i of the indicators, respectively; and a, b, c, and d are the numbers of the indicators, respectively.

We constructed a flood risk assessment index system for the YRDUA based on the "H–E–V–R" framework, the actual situation of the study area, the formation mechanisms of flood disasters, and the findings of relevant studies (Gain et al., 2015; Criado et al., 2019; Hsiao et al., 2021). We selected four first-level indicators (i.e., hazard, exposure, vulnerability, and resilience indices) and 19 second-level indicators. A detailed description of the flood risk assessment index system is presented in **Figure 4**.

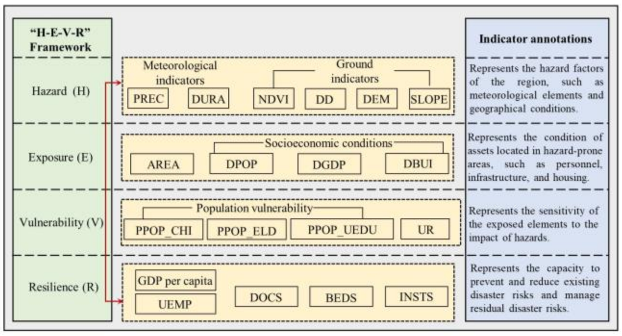

Figure 4: Flood risk assessment index system for the YRDUA based on the H–E–V–R framework.

Formatted

Formatted: Font: Times New Roman

Formatted

The hazard indicators consisted of six indices: Average annual precipitation (PREC), Annual Cumulative Heavy Rainfall Duration (DURA), Digital Elevation Model (DEM), SLOPE, Drainage Density (DD), and Normalized Difference Vegetation Index (NDVI~~) were selected as hazard indicators to evaluate the sensitivity of flood-prone environments; land~~). Rainfall is the primary factor leading to flooding, particularly extreme rainstorms caused by climate change. According to the Meteorological Bureau's definition, a heavy rainstorm event is characterized by rainfall of 50mm or more within 24 hours. DURA is defined as the total number of days with heavy rainstorm events occurring at all meteorological stations within the study area each year. The more days heavy rainstorms accumulate and the longer their duration, the greater the likelihood of flooding and other disaster events. DEM and SLOPE are important topographical indicators. Areas with low DEM and SLOPE values are generally more susceptible to flood threats. DD refers to the area of rivers or lakes per unit of land surface area and is a crucial indicator of a watershed's structural characteristics. It determines the watershed's capacity to withstand flooding. The higher the DD, the greater the likelihood of flooding and the higher the potential flood risk. Vegetation plays a role in water storage, retention, and infiltration. The lower the vegetation coverage, the weaker the buffering capacity, making it more likely for surface water to accumulate. The NDVI index measures the relative abundance of green vegetation, with values ranging from -1 to 1. The higher the value, the greater the vegetation coverage, and the lower the risk of flooding.

Land area (AREA), Population Density (DPOP), GDP Density (DGDP), and Building Density (DBUI) were selected as exposure indicators to ~~measure the degree of exposure of the natural environment or social system to flooding;~~assess the degree of vulnerability of both the natural environment and social systems to flooding. The land area for each administrative unit at the prefecture-level city is calculated individually. A larger land area corresponds to a greater extent exposed to flooding. DPOP and DGDP represent the concentration of population and assets, respectively. Areas with higher DPOP and DGDP are more susceptible to potential threats from pluvial flooding. DBUI, the ratio of total building area to total land area in a region, indicates the building density. A higher DBUI reflects greater exposure to flooding.

Vulnerability indicators focus more on the social aspects of flood disasters. This study selects four vulnerability indicators: Proportion of Child Population (PPOP_CHI), Proportion of Elderly Population (PPOP_ELD), Proportion of Uneducated Population (PPOP_UEDU), and Urbanization Rate (UR~~) were~~

~~selected as vulnerability indicators to reflect the vulnerability to flooding; GDP per capita (GDP),~~). Age is a key feature of social vulnerability, and both the population aged 0-14 and those over 65 are considered vulnerable groups, as these age groups are more susceptible to flood damage. The uneducated population generally has a weaker awareness of disaster risks and lower self-protection capacity, which makes this group more vulnerable to flooding. The urbanization rate refers to the proportion of the urban population in the total resident population of a region. This indicator is inversely related to flood vulnerability. In general, a higher urbanization rate indicates greater social development and stronger protective capacities, which can reduce vulnerability to flooding to some extent.

The resilience indicators selected in this study include Gross Domestic Product (GDP) per capita, Unemployment Rate (UEMP), Number of Doctors (DOCS), Number of Medical Institutions (INSTS), and Number of Hospital Beds (BEDS~~) were selected as resilience indicators. A detailed description of the flood risk assessment index system is presented in **Fig. 3**.~~). GDP per capita is the ratio of a region's GDP to its total resident population over a specified period, reflecting the region's economic condition. A higher GDP per capita indicates a more developed economy, which is associated with a greater capacity to recover quickly after a flooding event. The Unemployment Rate (UEMP) measures the proportion of the idle labor force, indirectly reflecting the stability of urban development. A high unemployment rate signals economic instability, which weakens the capacity to cope with floods and extends the time required for post-disaster recovery, thus impeding disaster response efforts. The indicators of DOCS, INSTS, and BEDS provide insights into a region’s healthcare and medical support capabilities. Areas with stronger healthcare systems are better positioned to manage flood risks and recover more effectively from such disasters.

Formatted: Font: 9 pt, Bold, German (Germany)

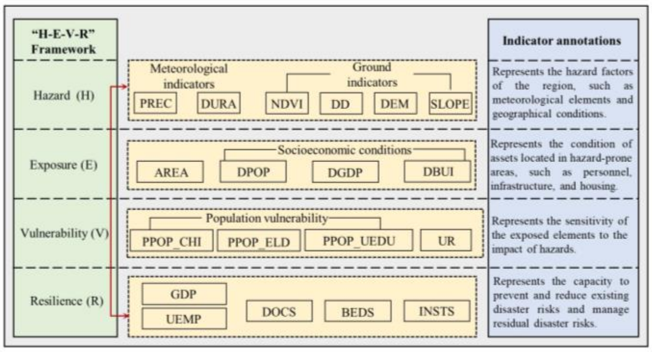

~~**Figure 3: Flood risk assessment index system for the YRDUA based on the H–E–V–R framework.**~~

Formatted: German (Germany)

2.~~4~~5 Flood risk calculation method based on AutoML

2.~~4~~5.1 Feature selection

~~The training sample dataset was generated based on flooded and non-flooded points in the study area.~~The flood inventory map in this paper was developed using inundation data from the Global Flood Database and flood disaster data from the EM-DAT database, supplemented by satellite and Google image interpretation and verified against existing historical flood records. The actual flood-affected areas were delineated based on flood traces from the inundation datasets and image interpretations. For this study, 278 flood inundation points were randomly selected within the inundation data range during the study period, and the location of each point was used as the basis for subsequent statistical analysis of flood events. The main factors affecting flood risk were considered during input feature selection. Rainfall and rainstorms are important factors that lead to floods, and flooding is closely related to topography, slope, vegetation cover, and hydrological conditions. Therefore, six indicator factors, namely PREC, DURA, DEM, SLOPE, NDVI, and DD, were selected as the input features of the model. To verify the model, 70% of the data in the sample were set as the training dataset and the remaining 30% of the data were set as the testing dataset through random sampling.

When the number of samples is small, data balancing is essential to ensure uniform sampling and reduce the deviations among the training, validation, and original datasets. Data balancing refers to the process of achieving a balanced distribution of data for each labeled category; it is particularly important when the number of observations in each class is significantly different. One way to address an imbalanced dataset is to oversample the minority classes. In this study, we assessed flood risk based on the identification of flooded point in the sample, which is essentially a binary classification problem; therefore, the output features are 0, i.e., negative categories (non-flooded points), versus 1, i.e., positive categories (flooded points). The processed dataset comprised 278 positive samples (flooded points) and 278 negative samples (non-flooded ~~point).~~points), with each label consisting of 278 points representing the entire dataset.

2.~~4~~5.2 Model training and hyperparameter optimization

Training samples were generated using the data from flooded and non-flooded points in the study area, and the Auto-Sklearn was used for model training, its principle is shown in **Figure 5**. The Auto-sklearn framework has multiple built-in machine learning algorithms. We selected 9 models that are more typical or have better performance in flood hazard research: random forest (RF), extreme gradient boosting (XGBoost), Light Gradient Boosting Machine (LightGBM), categorical feature boosting (CatBoost), ~~extra~~Extra trees, ~~decision~~Decision tree, ~~nearest neighbors,~~Nearest Neighbors, Multi-layer Perceptron (MLP) neural network, and ~~linear~~Linear Regression. The training and testing datasets were used to train the 9 machine learning models, and the hyperparameters were continuously adjusted and optimized.

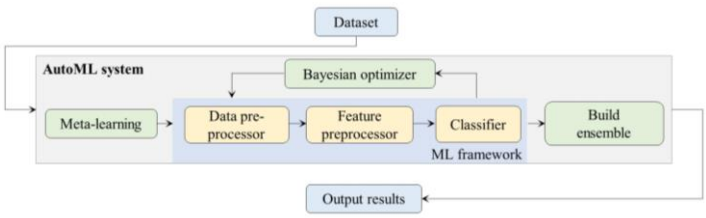

Figure 5: Principles of Auto-Sklearn

Hyperparameter optimization is an important step in ML model training. The aim of this step is to determine a hyperparameter combination to generate a ML model that performs well on a specific dataset and reduces the effect of the predefined loss function on a given dataset. In this study, we used a grid search strategy for optimization. For each set of hyperparameter combinations, k-fold cross-validation was used to evaluate the model and determine the hyperparameter combination of the optimal model that achieved the ~~highest prediction accuracy.~~best balance of Precision, Recall, and F1-score. Briefly, the training dataset was divided into K parts, of which one was selected as the test set and the rest were used as the training set. The cross-validation was repeated K times and the results were averaged K times. The model with the best average result among all models was selected as the optimal model, and the final classification prediction result was the output. In this study, we used 5-fold cross-validation.

2.~~4~~5.3 Performance evaluation

To better compare the ~~accuracy~~performance of the ~~14~~9 selected ML models in the Auto-Sklearn framework for flood risk assessment, multiple~~ accuracy~~ evaluation indicators were used to assess the test dataset. The following combinations of the true category of the sample point and the category predicted by the classifier were used: True Positive (TP)—the sample point is a flooded point, and the model classifier also predicts that it is a flooded point; True Negative (TN)—the sample point is a non-flooded point, and the model classifier also predicts that it is a non-flooded point; False Positive (FP)—the sample point is a ~~flooded point, and the model classifier mistakenly predicts that it is a non-flooded point; False Negative (FN)—the sample point is a~~ non-flooded point, and the model classifier mistakenly predicts that it is a flooded point~~.~~; False Negative (FN)—the sample point is a flooded point, and the model classifier mistakenly predicts that it is a non-flooded point. Therefore, four related indicators were selected: ~~Accuracy,~~ Precision, Recall and F1-score, and the consistency metric ~~kappa~~Kappa coefficient~~, the~~. The calculation ~~formula is as follows~~ formulas are given in Eq. ~~(2)~~(3), Eq. ~~(3), Eq.~~ (4), ~~Eq.(5), Eq. (6). A combination of multiple indicators can be used to better compare the performances of several models in the Auto-Sklearn framework for flood point identification and flood risk assessment. The equations for calculating the above indicators are shown below. The most intuitive precision performance indicator is accuracy. As the Auto-Sklearn framework uses data balancing to ensure adaptive balanced class distribution, the model with the highest accuracy value is the best performing model in flood point identification in this study.~~and Eq. (5):

$$\cancel{Accuracy = \frac{TP+TN}{TP+FP+TN+FN},} \quad \cancel{(2)}$$

$$\cancel{Precision = \frac{TP}{TP+FP},} \quad \cancel{(3)}$$

$$\cancel{Recall = \frac{TP}{TP+FN},} \quad \cancel{(4)}$$

$$\cancel{F1-score = \frac{2TP}{2TP+FP+FN}.} \quad \cancel{(5)}$$

$$Precision = \frac{TP}{TP+FP}, \tag{3}$$

$$Recall = \frac{TP}{TP+FN}, \tag{4}$$

$$F1-_{score} = \frac{2TP}{2TP+FP+FN}. \tag{5}$$

Formatted: Font: +Body Asian (等线)

Among the indicators, *~~Accuracy~~* ~~is determined based on the accuracy rate and can also be understood as the consistency of the prediction, indicating the degree of closeness or distance between the predicted category given by a set of data and its true category.~~ *Precision* ~~is the accuracy rate and~~ refers to the ~~degree of closeness or dispersion among the predicted categories.~~ ~~*Recall* is the recall rate and refers to the ability of the prediction result to~~ proportion of correctly ~~classify and identify the~~ predicted flooded points~~.~~ among all predicted flooded points, reflecting the model's ability to avoid false positives. *Recall* measures the proportion of correctly identified flooded points among all actual flooded points, representing the model's sensitivity. *F1-score* is the harmonic mean of Precision and Recall ~~and is equivalent to the comprehensive evaluation index of the precision and recall rates and can better reflect the~~, providing a balanced evaluation of both metrics and reflecting the overall recognition performance of the model.

Kappa coefficient is ~~an indicator of~~a statistical consistency ~~in statistics, it is~~metric used to measure ~~the effects of~~ classification~~, and it was~~ performance, which is calculated based on the confusion matrix of ~~the~~ true and predicted categories ~~in this study~~. Its value ~~range is~~ranges from [-1,~~-~~1]~~.~~: A ~~model with a low~~ Kappa value of 1 indicates ~~an unbalanced confusion matrix. Its formula is as Eq.~~perfect agreement, 0 means the classification is no better than random guessing, and negative values suggest the classification is worse than random prediction. *Kappa* is calculated using Eq. ~~(6)~~(6), ~~Eq.~~where P_e is given by Eq. ~~(7)~~ (7).

$$Kappa = \cancel{\frac{Accuracy - P_e}{1 - P_e}} ,$$

Formatted: Font: Italic

Formatted: Font: Italic

Formatted: Font: Italic

Formatted

Formatted: Font: Times New Roman

Formatted: Tab stops: 14.81 cm, Right

$$\frac{P_o - P_e}{1 - P_e}, \quad (6)$$

Formatted

$$\cancel{P_e = \frac{(TP+FP)+(TP+FN)+(TN+FN)+(TN+FP)}{(TP+FP+TN+FN)^2}, \quad (7)}$$

$$P_e = \frac{(TP+FP)(TP+FN)+(TN+FN)(TN+FP)}{(TP+FP+TN+FN)^2}, \quad (7)$$

where P_e represents the ~~accidental consistency~~expected agreement by chance.

Formatted: Font: Times New Roman

Combining multiple indicators allows for a more comprehensive evaluation of models within the Auto-Sklearn framework for flood point identification and flood risk assessment.

2.~~5~~6 Method for determining flood risk index weights based on AHP

2.~~5~~6.1 Establishing a hierarchical model

According to the decision-making objectives, factors, and applications in decision-making problems, the AHP can be divided from bottom to top into the target, criterion, and application layers. Among them, the target layer is the problem to be solved (i.e., final flood risk). The criterion layer is the intermediate link, including the factors to be considered and the decision making criteria. The factors can be divided into different evaluation indicators, including four first-level indicators (danger, exposure, vulnerability, and resilience) and their corresponding 19 second-level indicators. The criterion layer comprises various weight combination schemes linked to the target layer. The application layer is the final optional scheme and specific application of the decision. The final weight scheme and evaluation results of this study were applied to the YRDUA.

2.~~5~~6.2 Constructing the judgment matrix

After the hierarchical structure was established, a judgment matrix was constructed based on the relationship between the criteria and indicators. Different elements in the sublevel were compared pairwise, and the relative importances of all elements in the current layer and previous layer were compared. Typically, a pairwise comparison matrix is used as representative. In this study, we adopted the 1–9 scale method as the importance measurement standard. The importance comparison relationship is presented in **Table 2**, where the matrix element a_{ij} represents the comparison result of the ith element relative to the jth element.

Table 2: Pairwise comparison point-based rating scale of AHP.

Ranking	Importance Level
1	Equally important
3	*i* is slightly more important than *j*
5	*i* is much more important than *j*
7	*i* is very much more important than *j*
9	*i* is extremely important than *j*
2, 4, 6, 8	Intermediate value of two adjacent ~~judgements~~judgments
Reciprocal	Comparative ~~judgement~~judgment of j vs., $a_{ji} = 1/a_{ij}$

2.~~5~~6.3 Solving the eigenvector of the judgment matrix

Based on the judgment matrix, the square root method was used to solve the eigenvector and ~~eigenroot~~eigenvalue. The first step is to calculate the square root a_{ij} of the product of each row of the judgment matrix n, then normalize it, and finally calculate the maximum ~~eigenroot~~eigenvalue of the judgment matrix. The formula is as Eq. (8), Eq. (9), Eq~~. (10).~~ (10).

$$M_i = \sqrt[n]{\prod_{j=1}^{n} a_{ij}} , \quad (8)$$

$$W_i = \frac{M_i}{\sum_{i=1}^{n} M_i} ,$$

(9)

$$\lambda_{max} = \sum_{i=1}^{n} \frac{(AW)_i}{nW_i},$$

(10)

2.~~5~~6.4 Consistency check

After the eigenvector calculation is completed, a consistency test is required to reduce the subjectivity in the judgment matrix and enhance the scientific nature of the data and calculations. In a pairwise comparison matrix, consistency means that the decision-maker's judgments must exhibit logical coherence and transitivity. Specifically, if option A is considered more important than option B, and option B is considered more important than option C, then consistency requires that option A must also be judged more important than option C (Saaty, 1984).

The consistency indicator (CI) is used to measure the deviation of the judgment matrix from the consistency: the smaller the CI, the greater the consistency of the judgment matrix. When CI = 0, the judgment matrix is completely consistent. The CI calculation formula is as Eq. ~~(11)~~(11).

$$CI = \cancel{\frac{\lambda-n}{n-1}}$$

$$\frac{\lambda_{max}-n}{n-1}\cancel{,} \qquad (11)$$

To quantify the standard, the relative consistency (CR) index was further calculated as Eq. ~~(12)~~(12).

$$CR = \frac{CI}{RI}$$

$$\cancel{,} \qquad (12)$$

~~where~~Where average Random Consistency Index (RI) represents the average random consistency~~,~~ which ~~is~~depends only ~~related to~~on the order of the judgment matrix. The RI values ~~of~~for judgment matrices of order ~~1–10 are shown in **Table 3**~~1 to 10 are shown in **Table 3.**

Table 3: Consistency index (RI) for a randomly generated matrix.

n	1	2	3	4	5	6	7	8	9	10
RI	0.00	0.00	0.52	0.89	1.12	1.26	1.36	1.41	1.46	1.49

CR was determined based on the RI value. When CR < 0.1, the consistency of the judgment matrix is considered good. When CR > 0.1, the consistency of the judgment matrix is unacceptable, and the judgment matrix must be adjusted and modified. In such cases, the corresponding judgment matrix was further constructed, and the eigenvector and ~~eigenroot~~eigenvalue were calculated using the following formulas:

Finally, the judgment matrix that passed the consistency test was used to calculate the weights of the indicators at the different levels.

2.7 Determination of flood risk levels

The classification of flood risk levels often involves manually setting thresholds, which can introduce subjectivity and influence the accuracy of the risk assessment outcomes (Ma et al., 2022). To calculate the flood risk, we employed the natural breakpoint classification method, which groups data into classes based on natural divisions within the dataset (Lin et al., 2019). This method works by identifying points where the data distribution changes most significantly and dividing the data into ranges based on these breaks. Unlike clustering methods, which do not focus on the number and range of elements in each

Formatted: Tab stops: 14.81 cm, Right

Formatted: Font: 10 pt

Formatted: Font: 10 pt

group, the natural breakpoint method ensures that the range and number of elements in each group are as balanced as possible (Ma et al., 2022).

3 Results and discussion

3.1 Model flood risk results and evaluation

3.1.1 AutoML optimal model selection

In the experiment, 9 typical ML models under the Auto-Sklearn framework were used to process the sample dataset, with 70% of the sample set being used as the training dataset and 30% being used as the testing dataset. The results of the comparative analysis of the model performance based on the test dataset are presented in **Table 4**. A comprehensive analysis of the results on the testing data revealed that~~ the accuracy of the models followed the order of CatBoost (~~, in~~0.8960) = LightGBM (0.8960) > Extra Trees (0.8880) > other models > Nearest Neighbors. In~~ terms of ~~the precision index~~Precision, CatBoost had the highest value (0.9030), followed by~~ those of~~ LightGBM (0.8960) and Extra Trees (0.8893). Meanwhile, CatBoost had the highest recall rate of 0.8883, followed by that of Extra Trees at 0.8870. The probability thresholds for Precision, Recall, and F1-score range from [0,1], while the Kappa coefficient ranges from [-1,1]. The F1-score and Kappa coefficient of the CatBoost model were also markedly higher than those of the other models, reflecting the model's good consistency. A comprehensive comparison showed that the ~~accuracy, ~~precision, F1-score, and ~~kappa~~Kappa coefficient of the CatBoost model were the highest, with its ~~accuracy~~precision reaching 0.~~8960~~9030, indicating that the recognition and prediction ~~accuracy~~precision of the flooded points in the study area based on the CatBoost model were obviously better than those of other common machine learning models.

Since flood data often involve various environmental factors and complex interactions, the CatBoost model is highly effective at handling these intricate nonlinear relationships and feature interactions. Additionally, the model incorporates multiple regularization mechanisms during tree construction, which helps prevent overfitting and enhances the model's generalization capability. The results indicate that most models performed well on the training set, but their performance slightly declined on the test set, highlighting variations in generalization ability. CatBoost demonstrated strong robustness, achieving a Precision of 0.9319 on the training set and 0.9030 on the test set. Additionally, LightGBM and XGBoost showed relatively consistent performance between the training and test sets, suggesting better generalization. However, models such as Decision Tree and Nearest Neighbors exhibited a more significant performance drop in the test set, indicating a higher sensitivity to overfitting. To further evaluate overfitting, we used 5-fold cross-validation by comparing the performance of the training and testing sets. The experimental results indicate that while most models showed some performance decline on the test set, CatBoost maintained relatively stable performance, suggesting that the model does not exhibit significant overfitting and has good generalization ability.

Table 4: Comparative analysis of the performances of different ML models.

Models	Dataset~~Accuracy~~	Precision	Recall	F1-score	Kappa
CatBoost	Training set	0.9319	0.9307	0.9547	0.8614
~~CatBoost~~	~~0.8960~~Testing set	0.9030	0.8883	0.8960	0.7915
XGBoost	Training set	0.9017	0.8827	0.8818	0.8640
~~XGBoost~~	Testing set~~0.8640~~	0.8748	0.8640	0.8624	0.7256
LightGBM	~~0.8960~~Training set	0.~~8960~~9349	0.~~7890~~9307	0.~~8015~~9306	0.~~7324~~8616
	Testing set	0.8960	0.7890	0.8015	0.7324
Random Forest	Training set	0.8922	0.8747	0.8745	0.7484
~~Random Forest~~	~~0.8320~~Testing set	0.8482	0.8320	0.8309	0.6662
Extra Trees	Training set	0.8524	0.8240	0.8735	0.7695
~~Extra Trees~~	~~0.8880~~Testing set	0.8893	0.8870	0.8877	0.7751
Decision Tree	Training set	0.8886	0.8640	0.8621	0.8040
~~Decision Tree~~	~~0.8720~~Testing set	0.8810	0.8720	0.8708	0.7419
Linear Regression	Training set	0.8636	0.8533	0.8525	0.7073
~~Linear~~	~~0.8480~~Testing set	0.8682	0.8480	0.8450	0.6926
Nearest Neighbors	Training set	0.7301	0.7907	0.7987	0.6009
~~Nearest Neighbors~~	~~0.7440~~Testing set	0.7747	0.7440	0.7390	0.4937
MLP Neural Network	Training set	0.8998	0.8880	0.8873	0.7765
~~Neural Network~~	~~0.8480~~Testing set	0.8682	0.8480	0.8450	0.6926

By comparing the performances of the 9 models, we found that the CatBoost model was more effective in identifying flooded points. To further verify the excellent performance of the model, the receiver operating characteristic (ROC) curve and area enclosed by the coordinate axes (corresponding area under the curve [AUC] value) were plotted based on the test dataset to ~~determine the accuracy of~~assess the model's binary classification ~~effect~~effectiveness: the larger the AUC value, the ~~more accurate~~better the model ~~prediction~~distinguishes between classes. When AUC > 0.8, the model prediction effect is very good (Sinha et al., 2008). ~~The verification results are shown in~~ In this study, both micro- and macro-average ROC curves were plotted. The micro-average ROC curve aggregates the contributions of all classes to compute the average ROC curve, treating each instance equally, while the macro-average ROC curve computes the ROC curve for each class independently and then averages the results. These two methods are commonly used for multi-class classification problems, but in this study, they were used to give a more comprehensive comparison of model performance. The verification results are shown in **Figure 6**. The AUC value of the CatBoost model reached 0.91, guaranteeing the performance and prediction reliability of the CatBoost model. Based on this, the CatBoost model was selected to calculate the flood risk in the YRDUA.

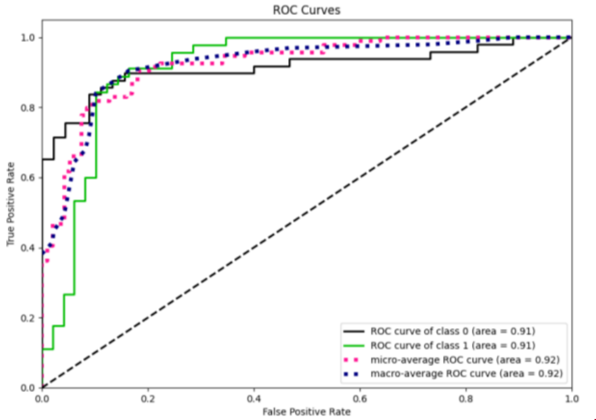

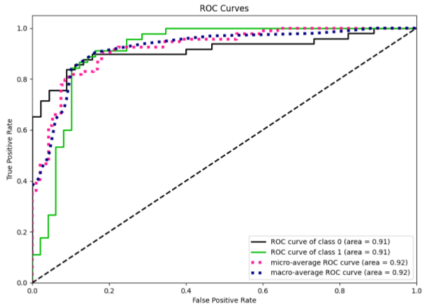

Figure 6: Receiver operating characteristic (ROC) curves and corresponding area under the curve (AUC) values of the CatBoost model.

3.1.2 ~~Analysis~~Importance and interpretability analysis of hazard factors

~~(1) Ranking of importance~~

~~Among~~To better understand the ~~six characteristic factors affecting flood risk, in order~~contribution of different hazard indicators to ~~clarify the main factors affecting~~ flood risk in the YRDUA, ~~this study quantifies the degree of importance of each risk indicator factor through the CatBoost model, and its~~we conducted both importance ranking ~~is~~analysis using the CatBoost model and interpretability analysis based on SHAP.

The CatBoost model was used to quantify the relative importance of six key hazard indicators. The results, shown in **Figure 7**~~. The results indicated that there are obvious differences in the degree of influence of the indicators on flood risk within the study area. DEM is the primary factor affecting flood risk, with an importance level of 68.55%, which far exceeds the other factors, which is also in line with the findings of many researchers within the region(Mei et al., 2021; Wan et al., 2013). Analyzing the main reasons, compared to higher terrain areas, low lying and relatively flat depressions become natural catchment areas. Additionally, since the main urban areas of the YRDUA predominantly consist of impervious surfaces, the surface runoff formed is difficult to infiltrate, further exacerbating the risk of water~~

~~accumulation and flooding in low-lying areas. At the same time, although rainfall is the primary disaster-causing factor for storm-induced flooding, the importance of the PREC is relatively low. Instead, the factor representing the DURA contributes 10.07% to the flood risk. This indicates that extreme weather events leading to heavy rainfall are more likely to cause considerable flood hazards.~~

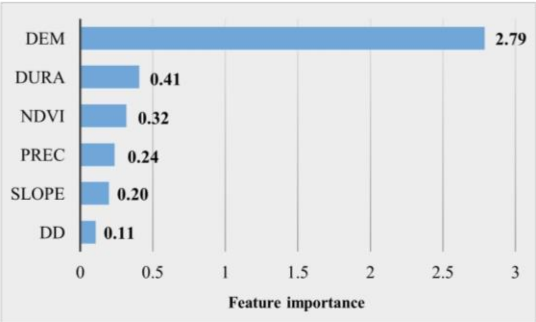

, reveal significant differences in their influence. DEM was identified as the most critical factor, contributing 68.55%, which far exceeds the other factors, which is also in line with the findings of many researchers within the region (Mei et al., 2021; Wan et al., 2013). Low-lying areas naturally function as water accumulation zones, increasing flood vulnerability. Additionally, urban areas in the YRDUA are dominated by impervious surfaces, limiting infiltration and exacerbating flood risks. While PREC is a primary factor in storm-induced flooding, its direct contribution to flood risk was relatively low compared to DURA, which accounted for 10.07%. This highlights that the persistence of extreme rainfall events is a stronger predictor of flood hazard than total annual precipitation.

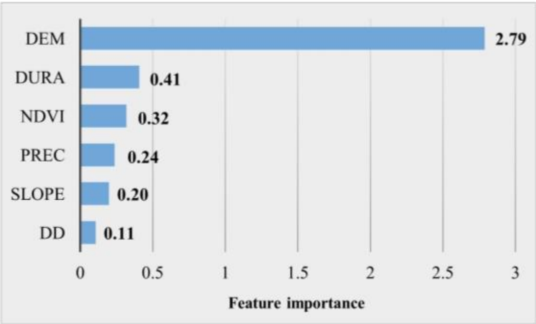

Figure 7: Importance Ranking of Hazard Factors Based on the CatBoost Model

Formatted: Font: Times New Roman

~~(2) SHAP interpretability analysis~~

To further analyze the interpretability of the model and understand the impact of individual flood hazard indicators on the model's classification results, this paper calculates Shapley Additive Explanations (SHAP) to indicate the contribution of each feature in the sample (Lundberg and Lee, 2017). ~~SHAP is a post-hoc interpretability method for models. Its core idea is to calculate the marginal contribution of features to the model's output(Wang et al., 2023a). For each prediction sample, the model produces a predicted value. The SHAP value is the value assigned to each feature in the sample, thereby determining the contribution and explaining the model. Fig. 7(a) shows the scatter plot generated by SHAP in the training set, which can be analyzed in conjunction with the connotations and significance of flood hazard characteristic factors. In the Fig. 7(a), each row represents a feature, and the horizontal axis is the SHAP value. The features are ranked according to the average absolute value of SHAP, which can be understood as the most important features. The wider areas indicate a large concentration of samples. Each point represents a sample, with redder colors indicating higher feature values and bluer colors indicating lower feature values. The results indicate that for risk features, DEM, SLOPE, and NDVI have varying degrees~~

~~of negative impact on flood risk, while DD, annual DURA, and PREC have varying degrees of positive impact on flood risk. This indicates that the higher DEM, the steeper SLOPE, and the greater the vegetation cover, the lower the flood hazard in the area. Conversely, higher DD, DURA, and higher PREC increase the flood hazard. At the same time, the absolute value of DEM is the highest, with SHAP values showing pronounced clustering below zero and a relatively dispersed sample distribution, indicating that the elevation factor is the most hazard factor affecting flooding~~SHAP, a game theory-based post-hoc interpretation method, quantifies the marginal impact of each feature on model predictions. The SHAP summary plot in **Figure 8** (a) ranks features based on their absolute SHAP values, consistent with the CatBoost importance ranking. Each row represents a feature, where red indicates higher feature values and blue indicates lower values. The results show that DEM, SLOPE, and NDVI negatively impact flood risk, meaning that higher elevation, steeper slopes, and greater vegetation coverage reduce flood hazards. In contrast, DD, DURA, and PREC positively impact flood risk, indicating that higher drainage density, longer durations of extreme rainfall, and increased precipitation levels contribute to higher flood hazards. Among these, DEM has the highest absolute SHAP value, with a strong clustering below zero, reinforcing its dominant role in flood risk determination.

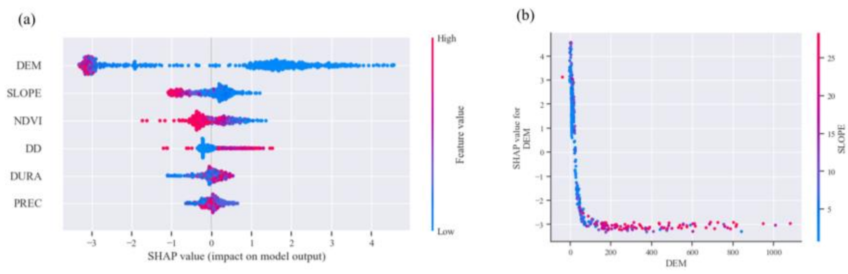

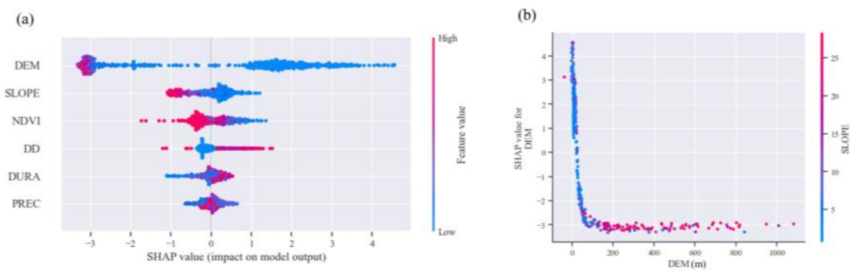

Figure 8: (a) Scatter Plot of Hazard Indicators from SHAP Analysis. (b) SHAP Dual Dependence Analysis of Elevation and Slope Factors.

To directly capture the interaction effects between paired indicator factors, this study used SHAP interaction values based on game theory, ensuring consistency while also explaining the interaction effects of individual predictions. For the DEM feature, which had the highest importance in the SHAP analysis, the factor most strongly correlated with it was SLOPE. Therefore, to illustrate how one feature interacts with another to affect the model training results, this study used DEM and SLOPE as examples to plot the SHAP interaction scatter plot, representing the dependency of the DEM feature. The results are shown in **Figure 8** (b). This dependency plot takes the form of a logarithmic function, indicating that as DEM increases, the flood hazard decreases. Additionally, the slope has a negative effect on the flood hazard in relation to elevation; that is, at lower elevations and gentler slopes, the flood hazard is greater.

3.1.3 Determination of flood risk index weights

A judgment matrix was constructed for 19 indicator factors. A hazard index was constructed based on feature importance calculated using AutoML. The exposure, vulnerability, and resilience indicators were determined based on existing literature and relevant expert scores (Hsiao et al., 2021). Combined with the actual characteristics of the YRDUA, the 1–9 scale method was used to compare item-by-item any two indicators and determine their relative importances and assign weights. Finally, the judgment matrix results were tested for consistency, and the CR value was 0.0058, i.e., << 0.100, indicating that the results passed the consistency test and that the flood risk index weight values calculated using the AHP were acceptable. The specific indicator weights and ~~attribute representations of~~ their corresponding impacts on flood risk are shown in ~~Table 5~~**Table 5**. The "Attribute" column represents the impact of each indicator on flood risk, with "+" indicating a positive impact on flood risk and "-" indicating a negative impact on flood risk.

Table 5: Flood risk index weights.

Dimension	Indicator	Unit	Attribute	Weight
Hazard (0.4798)	PREC	mm	+	4%
	DURA	Day	+	10.8%
	NDVI		-	7.6%
	DEM	km	-	22.99%
	SLOPE	°	-	6.4%
Exposure (0.1083)	DD	km/km²	+	3.2%
	AREA	km²	+	1.1%
	DPOP	people/km²	+	4.32%
	DGDP	10,000 yuan/km²	+	3.84%
	DBUI	km²	+	1.16%
Vulnerability (0.1312)	PPOP_CHI	%	+	4.92%
	PPOP_ELD	%	+	3.04%
	PPOP_UEDU	%	+	2.11%
	UR	%	-	2.05%
Resilience (0.2807)	GDP per capita	100 million yuan/10,000 People	-	4.43%
	UEMP	%	+	5.04%
	DOCS	Per person	-	4.13%
	INSTS	Each	-	0.45%
	BEDS	Per bed	-	6.28%

The weighted results reflect the degrees of influence of the different indicator factors on flood risk. Danger was the decisive factor affecting flood risk, with a weight of 0.4798, followed by resilience and vulnerability. Exposure had a relatively low impact on flood risk. In terms of danger, the topography and DURA were the main factors affecting the occurrence of flooding. These two indicators determined the characteristics of flood disasters in the YRDUA from the perspective of disaster-prone environments and driving factors, respectively. In terms of exposure, the YRDUA is a typical area with rapid social, economic, and population growths in China. High population and GDP densities increase the risk of flood exposure. In addition, the uneven age distribution and education levels of the population are important social factors affecting the risk of flood disasters in urban agglomerations. In terms of resilience, improving health and medical infrastructure, developing the regional economy, and reducing unemployment rates are conducive to improving the overall disaster response capacity of the region and reducing the risk of flood disasters in the YRDUA.

3.1.4 Model results verification

Based on CatBoost under the AutoML framework and AHP, the levels of ~~danger~~flood hazard, exposure, vulnerability, and resilience were calculated for floods in the YRDUA and the spatial distribution of flood risks in the region was obtained according to the weights determined by the model. Combined with the natural breakpoint classification method, a flood risk zoning map of the YRDUA was constructed. The extracted flood points were superimposed on the map to verify whether the model exhibited good flood risk assessment capabilities. The results are shown in **Figure 9**, indicating that the distribution of flood points was consistent with the distribution of high and medium-to-high risk areas in the region, with the model assessment results corresponding well with the actual flooding situation. To specifically illustrate the correspondence of the results, the proportion of flood points distributed in high and medium-to-high risk areas was quantitatively calculated. The obtained value was 87.45%, indicating that the flood risk assessment results of the model in this study were highly credible, and subsequent analysis could be conducted.

As shown in **Figure 9**, the high and medium-to-high risk areas in the YRDUA were mainly located in the northern part of the region, concentrated in Chizhou, Anqing, Ma'anshan, and Xuancheng Cities in Anhui Province, Yancheng and Yangzhou Cities in Jiangsu Province, and Taizhou City in Zhejiang Province. Meanwhile, most areas of Hangzhou City had the lowest risk. The flood risks in cities such as Shanghai, Nanjing, and Jinhua were also relatively low. The overall analysis showed that the flood risk in the study area was low in the southwest and high in the northeast, determined largely by natural terrain and meteorological factors. The spatial distribution of the flood hazard class was similar to the distribution of flood risks; exposure decreased stepwise from Shanghai to the surrounding areas, reflecting that densely populated and economically developed cities have higher exposure. Areas with higher vulnerability were mainly concentrated in Chizhou, Anqing, Xuancheng, Chuzhou, and Yancheng Cities. The number of vulnerable people in these cities was relatively high. Vulnerability has aggravated the flood risks in Chizhou and Anqing Cities on the basis of flood risk. Meanwhile, Shanghai had the best resilience performance, followed by those of Hangzhou, Suzhou, and Nanjing Cities, greatly lessening the flood risks in these cities.

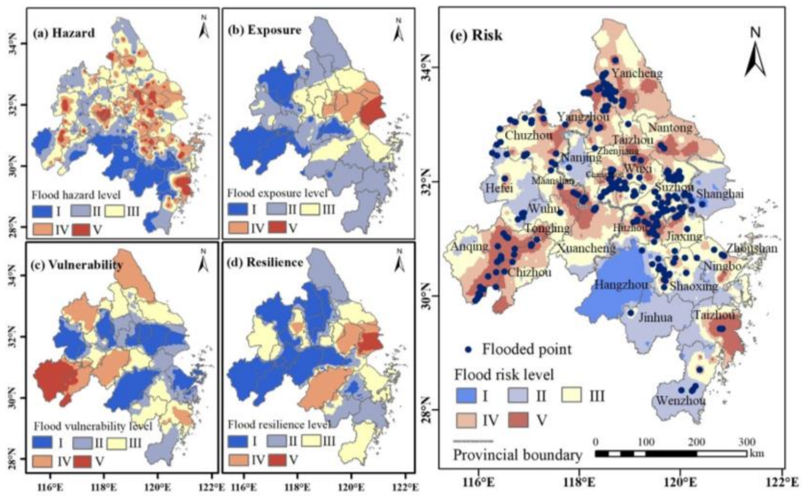

Figure 9: Flood risk level distribution and verification results based on a flood risk assessment model. The flood hazard, exposure, vulnerability, and resilience of the YRDUA were calculated using CatBoost under the AutoML framework and AHP. The flood hazard level (a), flood exposure level (b), flood vulnerability level (c), flood resilience level (d), and flood risk spatial distribution (e) were derived through natural breaks classification in ArcGIS software based on model-determined weights, resulting in a flood risk zoning map for the YRDUA.

3.2 Analysis of changes in the spatiotemporal characteristics of flood risk

The flood risk results for the YRDUA from 1990 to 2020 were obtained based on the flood risk assessment model proposed in this study. The differences in flood risk among cities in the YRDUA over the past few decades are primarily due to a complex interplay of various factors, including geographic and climatic conditions, urbanization processes, socio-economic factors, ecological changes, and historical flood events. The topography and precipitation patterns of different cities affect their capacity for rainwater drainage and accumulation, while urbanization leads to an increase in impervious surfaces and variations in infrastructure development, impacting flood management capabilities. Additionally, differences in DPOP, economic development levels, and flood management policies can exacerbate flood risk. Furthermore, the increasing frequency of extreme weather events due to climate change further elevates flood risk. These factors determine the varying levels of flood risk among cities within the YRDUA.

As the interannual difference in flood risk in the region was small and the change response was weak, we selected the flood risk results for 1990, 2000, 2010, and 2020 to analyze the changes in the spatiotemporal pattern. In this analysis, variables such as PREC and DURA exhibit clear temporal variability, as they change year by year due to weather patterns. However, other factors like DEM, SLOPE, NDVI, and urbanization indicators such as DPOP and GDP are spatial variables that do not exhibit direct temporal changes, but their effects on flood risk are influenced by changing socio-economic and ecological conditions.

Regarding spatial patterns (**Figure 10**), the flood risk in the YRDUA showed clear spatial heterogeneity. The southwestern part of the study area and Shanghai have shown low flood risks over the past 30 years, whereas the central and northern parts of the region have been more likely to face flood risks depending on the natural conditions, population, economic conditions, and recovery capacity of the region. Regarding temporal patterns, from 1990 to 2010, areas with high and medium-to-high risk decreased markedly. By 2010, most of the YRDUA (except for a few areas) was in a state of medium risk or below, with the southwestern region exhibiting a large range of low risk levels. The corresponding areas for each risk level are shown in **Figure 11**. From 1990 to 2010, areas of low and low-to-medium risk levels gradually increased, maximizing in 2010, whereas areas of medium risk and above continued to decrease. By 2020, the number of high-risk areas for flooding increased. There is a tendency for areas of medium-to-high risk in the central region to shift towards high-risk areas in 2020, as compared to the state in 1990. Meanwhile, high-risk areas for floods also appeared in Chizhou and Anqing Cities in Anhui Province, which was mainly due to the intensification of extreme weather, unbalanced population distribution, and rapid economic development in recent years.

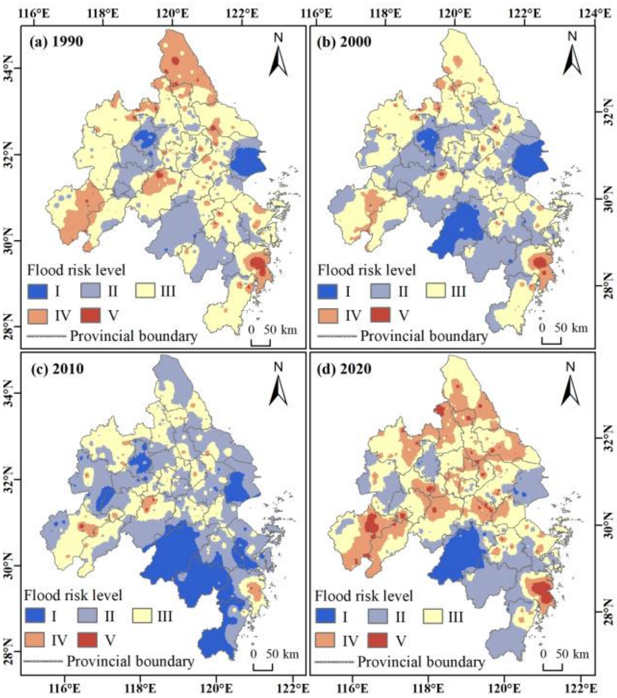
(a) 1990
(b) 2000
(c) 2010
(d) 2020
Flood risk level
I
II
III
IV
V
Provincial boundary
0 50 km
N
116°E
118°E
120°E
122°E
124°E
28°N
30°N
32°N
34°N

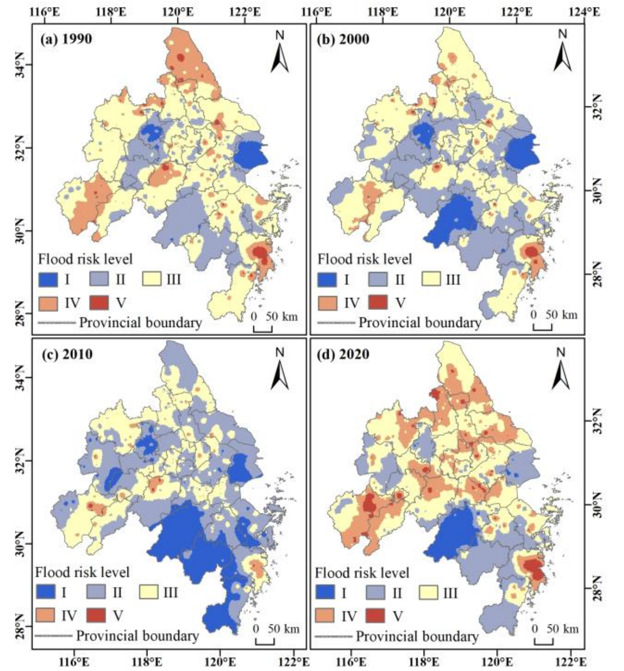

Figure 10: Spatial distributions of flood risk in the YRDUA in different years during 1990–2020.

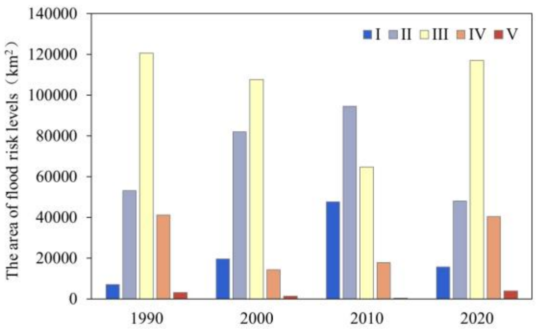

Figure 11: Areas at different levels of flood risk in the YRDUA in different years during 1990–2020.

To further analyze the changes in flood risk in the region, we calculated the change rate of the area of different risk levels every 10 years and the overall change rate over 30 years. The interannual rate of change was expressed ~~as follows:~~in Eq. (13).

$$R_{l,ij} = \frac{Risk_{l,j} - Risk_{l,i}}{Risk_{l,i}} \times 100\% \tag{13}$$

where $R_{l,ij}$ is the rate of change of the flood risk area of a certain level l in a certain year, i and j are different years, and $Risk_{l,j}$ and $Risk_{l,j}$ are the areas corresponding to the flood risk of this level in different years.

The interannual variation rate of the flood risk is shown in ~~Table 6.~~**Table 6**. Results showed that the interannual variation between the areas of low and high risk was relatively large. The low~~–~~-risk area maximized in 2010, and both R $_{2000–1990}$ and R $_{2010–2000}$ showed a positive variation rate. The high~~–~~-risk area showed the largest interannual variation rate from 2010 to 2020, reaching 12.~~218~~22% and causing the high~~–~~-risk flood area in 2020 to spread, resulting in a large high~~–~~-risk area.

Table 6: Interannual change rates of flood risk areas of different levels~~.~~ (expressed as percentages).

	$R_{2000\text{-}1990}$	$R_{2010\text{-}2000}$	$R_{2020\text{-}2010}$	$R_{2020\text{-}1990}$
I	1.~~766~~77%	1.~~443~~44%	-0.~~672~~67%	1.~~213~~21%
II	0.~~543~~54%	0.~~152~~15%	-0.~~491~~49%	-0.~~096~~10%
III	-0.~~106~~11%	-0.440%	0.81%	-0.~~029~~03%
IV	-0.~~653~~65%	0.~~252~~25%	1.~~254~~25%	-0.02%
V	-0.~~528~~53%	-0.~~796~~80%	12.~~218~~22%	0.~~274~~27%

Analyzing the flood risk of the entire urban agglomeration does not reveal the spatial scale effect of flood risk, nor does it consider the correlation and impact of flood risk at different spatial scales. To reflect the distribution of and changes in flood risk at different spatial scales within the region, the risk intensity of different provinces was further analyzed, and the results are shown in **Figure 12**, respectively. In **Figure 12**, the average flood risk reflects the differences in risk development of the provincial administrative

Formatted: Tab stops: 14.81 cm, Right

Formatted: Font: 10 pt (×26)

units in Shanghai, Anhui, Zhejiang, and Jiangsu in terms of time and space. Overall, all administrative units in the YRDUA exhibited the highest flood risk in 2020, and the overall risk trend increased. At the provincial level, Shanghai's flood risk was consistently low, showing a trend of first decreasing from 0.152 in 1990 to 0.123 in 2000 and then gradually increasing to 0.311 in 2020. Among the other three provinces, Jiangsu and Anhui had relatively high flood risks, reaching 0.525 and 0.516, respectively, in 2020, whereas Zhejiang had a relatively low flood risk, which remained stable between 1990 and 2010, with no distinct changes.

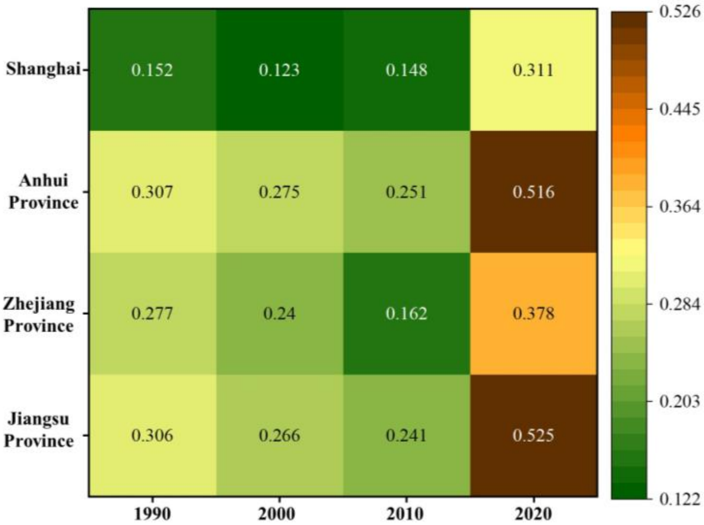

Figure 12: Distribution of Average Flood Risk in Each Province of the Yangtze River Delta Urban Agglomeration from 1990 to 2020

Formatted: Font: 9 pt, Bold

4 Conclusion

Flood risk assessment at the scale of urban agglomeration is a hot research topic in the field of disaster prevention and mitigation. In this study, the flood risk assessment indexes for YRDUA were determined in different dimensions of danger, exposure, vulnerability and resilience, and a flood risk assessment model based on AutoML and AHP was constructed to study the changes of spatial and temporal characteristics of flood risk in the region in the last 30 years from 1990 to 2020, aiming to provide scientific basis for the prevention and resilience of the YRDUA. The main conclusions of this study are as follows:

(1) In the flood risk calculation, the CatBoost model has the highest ~~Accuracy, ~~Precision, F1-score, and Kappa, and its ~~Accuracy~~Precision can reach 0.~~8960~~9030. Further analysis of the ROC curve and the corresponding AUC value of the model shows that its AUC value is 0.91, which indicates that the CatBoost model has the best performance and prediction reliability. Therefore, the CatBoost model was selected to calculate the flood risk in the YRDUA.

(2) Using the flood risk assessment model based on AutoML and AHP to obtain the flood risk of the YRDUA, superimposed on the flooded point data for comparative analysis, we found that the distribution of flooded points in the study area is basically consistent with the distribution of high and medium-to-high risk areas of flooding, and the proportion of the distribution of the quantification of its distribution is 87.45%, which indicates that the model in this study has a good performance and credibility regarding the assessment of flood risk.

(3) The spatial distribution of flood risk in the YRDUA during the 30-year study period shows obvious heterogeneity, with the southwestern part of the region and Shanghai City having a low flood risk, whereas the north-central part of the region faces a relatively high probability of flood risk. Between 1990 and 2010, there was a substantial decrease in the high and medium-to-high risk flood zones; yet by 2020, there was an increase in the high~~-~~-risk flood zones. There is a tendency for the medium-to-high risk area in the center of the region to shift to a high-risk area, whereas high~~-~~-risk areas also occur in the cities of Chizhou and Anqing in Anhui Province.

(4) All administrative units of the ~~YRD urban agglomeration~~YRDUA exhibited the highest flood risk in 2020, with an overall trend of increasing risk. At the provincial level, Jiangsu and Anhui Provinces possess relatively high flood risks, whereas Zhejiang Province has a relatively low flood risk.

(5) The findings of this study provide valuable insights for flood risk management and policy-making. The flood risk maps generated in this study can serve as a scientific basis for urban planning, infrastructure development, emergency response, and disaster prevention strategies. By integrating these risk assessments into decision-making processes, government agencies and urban planners can optimize flood prevention measures and enhance regional resilience. Furthermore, the AutoML framework used in this study can be applied to other regions for flood risk assessment and can be integrated with future climate change scenarios to enable long-term forecasting and proactive disaster mitigation strategies.

Data availability.

Data will be made available on request.

Competing interests.

The authors declare that they have no competing financial interests or personal relationships that may have influenced the work reported in this study.

Author contributions.

Yu Gao: Writing - original draft preparation, Validation, Software, Methodology, Conceptualization **Haipeng Lu:** Writing-review & editing, Visualization, Supervision, Formal analysis. **Yaru Zhang:** Methodology, Formal analysis. **Hengxu Jin:** Writing - review & editing, Methodology. **~~Suai~~Shuai Wu:** Software, Formal analysis. **Yixuan Gao:** Visualization, Software. **Shuliang Zhang:** Writing-review & editing, Resources, Project administration, Funding acquisition, Conceptualization .

Acknowledgements

This study was supported by the National Natural Science Foundation of China (Grant ~~Nos42271483~~Nos. 42271483 and 42071364) and Jiangsu Provincial Natural Resources Science and Technology Project (JSZRKJ202405). We would like to thank Editage (www.editage.cn) for English language editing.

References

Abu-Salih, B., Wongthongtham, P., Coutinho, K., Qaddoura, R., Alshaweesh, O., and Wedyan, M.: The development of a road network flood risk detection model using optimised ensemble learning, Eng. Appl. Artif. Intell., 122, 106081, https://doi.org/10.1016/j.engappai.2023.106081, 2023.

Adnan, R. M., Yuan, X., Kisi, O., and Anam, R.: Improving Accuracy of River Flow Forecasting Using LSSVR with Gravitational Search Algorithm, Advances in Meteorology, 2017, 1–23, https://doi.org/10.1155/2017/2391621, 2017.

Anon: Identification of sensitivity indicators of urban rainstorm flood disasters: A case study in China, J. Hydrol., 599, 126393, https://doi.org/10.1016/j.jhydrol.2021.126393, 2021.

Aven, T.: Risk assessment and risk management: Review of recent advances on their foundation, European Journal of Operational Research, 253, 1–13, https://doi.org/10.1016/j.ejor.2015.12.023, 2016.

Bostan, P. A., Heuvelink, G. B. M., and Akyurek, S. Z.: Comparison of regression and kriging techniques for mapping the average annual precipitation of Turkey, Int. J. Appl. Earth Obs. Geoinf., 19, 115–126, https://doi.org/10.1016/j.jag.2012.04.010, 2012.

Consuegra-Ayala, J. P., Gutiérrez, Y., Almeida-Cruz, Y., and Palomar, M.: Intelligent ensembling of auto-ML system outputs for solving classification problems, Inform. Sci., 609, 766–780, https://doi.org/10.1016/j.ins.2022.07.061, 2022.

Criado, M., Martínez-Graña, A., San Román, J. S., and Santos-Francés, F.: Flood risk evaluation in urban spaces: The study case of Tormes River (Salamanca, Spain), International journal of environmental research and public health, 16, 5, 2019.

Ding, T., Chen, J., Fang, Z., and Chen, J.: Assessment of coordinative relationship between comprehensive ecosystem service and urbanization: A case study of Yangtze River Delta urban Agglomerations, China, Ecol. Indic., 133, 108454, https://doi.org/10.1016/j.ecolind.2021.108454, 2021.

Donegan, H. A., Dodd, F. J., and McMaster, T. B. M.: A New Approach to Ahp Decision-Making, Journal of the Royal Statistical Society: Series D (The Statistician), 41, 295–302, https://doi.org/10.2307/2348551, 1992.

Echendu, A. J.: The impact of flooding on Nigeria's sustainable development goals (SDGs), Ecosyst. Health Sustainability, 6, 1791735, https://doi.org/10.1080/20964129.2020.1791735, 2020.

~~Fabian, P.: Scikit-learn: Machine learning in Python, Journal of machine learning research 12, 2825, 2011.~~

Fernández, D. S. and Lutz, M. A.: Urban flood hazard zoning in Tucumán Province, Argentina, using GIS and multicriteria decision analysis, Eng. Geol., 111, 90–98, 2010.

Gain, A. K., Mojtahed, V., Biscaro, C., Balbi, S., and Giupponi, C.: An integrated approach of flood risk assessment in the eastern part of Dhaka City, Nat. Hazards, 79, 1499–1530, https://doi.org/10.1007/s11069-015-1911-7, 2015.

Gu, C., Hu, L., Zhang, X., Wang, X., and Guo, J.: Climate change and urbanization in the Yangtze River Delta, Habitat Int., 35, 544–552, https://doi.org/10.1016/j.habitatint.2011.03.002, 2011.

Guan, X., Yu, F., Xu, H., Li, C., and Guan, Y.: Flood risk assessment of urban metro system using random forest algorithm and triangular fuzzy number based analytical hierarchy process approach, Sustainable Cities and Society, 109, 105546, https://doi.org/10.1016/j.scs.2024.105546, 2024.

Gudiyangada Nachappa, T., Tavakkoli Piralilou, S., Gholamnia, K., Ghorbanzadeh, O., Rahmati, O., and Blaschke, T.: Flood susceptibility mapping with machine learning, multi-criteria decision analysis and ensemble using Dempster Shafer Theory, Journal of Hydrology, 590, 125275, https://doi.org/10.1016/j.jhydrol.2020.125275, 2020.

Guo, Y., Quan, L., Song, L., and Liang, H.: Construction of rapid early warning and comprehensive analysis models for urban waterlogging based on AutoML and comparison of the other three machine learning algorithms, J. ~~Hydrol~~Hydrology., 605, 127367, 2022a.

Guo, Y., Quan, L., Song, L., and Liang, H.: Construction of rapid early warning and comprehensive analysis models for urban waterlogging based on AutoML and comparison of the other three machine learning algorithms, J. ~~Hydrol~~Hydrology., 605, 127367, https://doi.org/10.1016/j.jhydrol.2021.127367, 2022b.

He, X., Zhao, K., and Chu, X.: AutoML: A survey of the state-of-the-art, Knowledge-Based Systems, 212, 106622, https://doi.org/10.1016/j.knosys.2020.106622, 2021.

Hsiao, S.-C., Chiang, W.-S., Jang, J.-H., Wu, H.-L., Lu, W.-S., Chen, W.-B., and Wu, Y.-T.: Flood risk influenced by the compound effect of storm surge and rainfall under climate change for low-lying coastal areas, Science of the total environment, 764, 144439, 2021.

Jordan, M. and Mitchell, T.: Machine learning: Trends, perspectives, and prospects, Science, 349, 255–260, https://doi.org/10.1126/science.aaa8415, 2015.

Kanani-Sadat, Y., Arabsheibani, R., Karimipour, F., and Nasseri, M.: A new approach to flood susceptibility assessment in data-scarce and ungauged regions based on GIS-based hybrid multi criteria decision-making method, J. Hydrol., 572, 17–31, https://doi.org/10.1016/j.jhydrol.2019.02.034, 2019.

Kazienko, P., Lughofer, E., and Trawinski, B.: Editorial on the special issue "Hybrid and ensemble techniques in soft computing: recent advances and emerging trends," Soft Comput., 19, 3353–3355, https://doi.org/10.1007/s00500-015-1916-x, 2015.

Khadka, D., Babel, M. S., and Kamalamma, A. G.: Assessing the Impact of Climate and Land-Use Changes on the Hydrologic Cycle Using the SWAT Model in the Mun River Basin in Northeast Thailand, Water, 15, 3672, https://doi.org/10.3390/w15203672, 2023.

Khosravi, K., Shahabi, H., Pham, B. T., Adamowski, J., Shirzadi, A., Pradhan, B., Dou, J., Ly, H.-B., Gróf, G., Ho, H. L., Hong, H., Chapi, K., and Prakash, I.: A comparative assessment of flood susceptibility modeling using Multi-Criteria Decision-Making Analysis and Machine Learning Methods, J. Hydrol., 573, 311–323, https://doi.org/10.1016/j.jhydrol.2019.03.073, 2019.

Lang, M., Barriendos, M., Llasat, M. C., Francés, F., Ouarda, T., Thorndycraft, V., Enzel, Y., Bardossy, A., Coeur, D., and Bobée, B.: Use of Systematic, Palaeoflood and Historical Data for the Improvement of Flood Risk Estimation. Review of Scientific Methods, Nat. Hazards, 31, 623–643, https://doi.org/10.1023/B:NHAZ.0000024895.48463.eb, 2004.

Li, J., Cheng, K., Wang, S., Morstatter, F., Trevino, R. P., Tang, J., and Liu, H.: Feature Selection: A Data Perspective, ACM Comput. Surv., 50, 94:1-94:45, https://doi.org/10.1145/3136625, 2017.

Lin, L., Wu, Z., and Liang, Q.: Urban flood susceptibility analysis using a GIS-based multi-criteria analysis framework, Nat Hazards, 97, 455–475, https://doi.org/10.1007/s11069-019-03615-2, 2019.

Liu Jiafu and Zhang Bai: Progress of Rainstorm Flood Risk Assessment, ~~地理科学~~ Geographical science, 35, 346–351, https://doi.org/10.13249/j.cnki.sgs.2015.03.013, 2015.

Lu, H., Lu, X., Jiao, L., and Zhang, Y.: Evaluating urban agglomeration resilience to disaster in the Yangtze Delta city group in China, Sustainable Cities and Society, 76, 103464, 2022.

Lundberg, S. M. and Lee, S.-I.: A Unified Approach to Interpreting Model Predictions, in: Advances in Neural Information Processing Systems, 2017.

Ma, C., Chen, Z., Zhao, K., Xu, H., and Qi, W.: Improved urban flood risk assessment based on spontaneous-triggered risk assessment conceptual model considering road environment, Journal of Hydrology, 608, 127693, https://doi.org/10.1016/j.jhydrol.2022.127693, 2022.

Mahmoud, S. H. and Gan, T. Y.: Urbanization and climate change implications in flood risk management: Developing an efficient decision support system for flood susceptibility mapping, Science of The Total Environment, 636, 152–167, https://doi.org/10.1016/j.scitotenv.2018.04.282, 2018.

~~Mei, C., Liu, J., Wang, H., Shao, W., Yang, Z., Huang, Z., Li, Z., and Li, M.: Flood risk related to changing rainfall regimes in arterial traffic systems of the Yangtze River Delta, Anthropocene, 35, 100306, https://doi.org/10.1016/j.ancene.2021.100306, 2021.~~

Mia, Md. U., Rahman, M., Elbeltagi, A., Abdullah-Al-Mahbub, Md., Sharma, G., Islam, H. M. T., Pal, S. C., Costache, R., Islam, A. R. Md. T., Islam, M. M., Chen, N., Alam, E., and Washakh, R. M. A.:

Sustainable flood risk assessment using deep learning-based algorithms with a blockchain technology, Geocarto International, 38, 1–29, https://doi.org/10.1080/10106049.2022.2112982, 2023.

Milanesi, L., Pilotti, M., and Ranzi, R.: A conceptual model of people's vulnerability to floods, Water Resources Res., 51, 182–197, https://doi.org/10.1002/2014WR016172, 2015.

Mirzaei, S., Vafakhah, M., Pradhan, B., and Alavi, S. J.: Flood susceptibility assessment using extreme gradient boosting (EGB), Iran, Earth Sci. Inf., 14, 51–67, https://doi.org/10.1007/s12145-020-00530-0, 2021.

Mishra, K. and Sinha, R.: Flood risk assessment in the Kosi megafan using multi-criteria decision analysis: A hydro-geomorphic approach, Geomorphology, 350, 106861, https://doi.org/10.1016/j.geomorph.2019.106861, 2020.

Morales-Torres, A., Escuder-Bueno, I., Andrés-Doménech, I., and Perales-Momparler, S.: Decision Support Tool for energy-efficient, sustainable and integrated urban stormwater management, Environmental Modelling & Software, 84, 518–528, https://doi.org/10.1016/j.envsoft.2016.07.019, 2016.

Munim, Z. H., Sørli, M. A., Kim, H., and Alon, I.: Predicting maritime accident risk using Automated Machine Learning, Reliab. Eng. Syst. Saf., 248, 110148, https://doi.org/10.1016/j.ress.2024.110148, 2024.

Nagarajah, T. and Poravi, G.: A Review on Automated Machine Learning (AutoML) Systems, in: 2019 IEEE 5th International Conference for Convergence in Technology (I2CT), 2019 IEEE 5th International Conference for Convergence in Technology (I2CT), 1–6, https://doi.org/10.1109/I2CT45611.2019.9033810, 2019.

Nayak, P. C., Sudheer, K. P., Rangan, D. M., and Ramasastri, K. S.: A neuro-fuzzy computing technique for modeling hydrological time series, J. Hydrol., 291, 52–66, 2004.

Özdemir, H., Baduna Koçyiğit, M., and Akay, D.: Flood susceptibility mapping with ensemble machine learning: a case of Eastern Mediterranean basin, Türkiye, Stoch. Env. Res. Risk A., 37, 4273–4290, https://doi.org/10.1007/s00477-023-02507-z, 2023.

Pham, B. T., Luu, C., Dao, D. V., Phong, T. V., Nguyen, H. D., Le, H. V., von Meding, J., and Prakash, I.: Flood risk assessment using deep learning integrated with multi-criteria decision analysis, Knowledge-Based Systems, 219, 106899, https://doi.org/10.1016/j.knosys.2021.106899, 2021.

Raschka, S.: Model Evaluation, Model Selection, and Algorithm Selection in Machine Learning, https://doi.org/10.48550/arXiv.1811.12808, 10 November 2020.

Rashidi Shikhteymour, S., Borji, M., Bagheri-Gavkosh, M., Azimi, E., and Collins, T. W.: A novel approach for assessing flood risk with machine learning and multi-criteria decision-making methods, Appl. Geogr., 158, 103035, https://doi.org/10.1016/j.apgeog.2023.103035, 2023.

Saaty, T. L.: The Analytic Hierarchy Process: Decision Making in Complex Environments, in: Quantitative Assessment in Arms Control: Mathematical Modeling and Simulation in the Analysis of Arms Control Problems, edited by: Avenhaus, R. and Huber, R. K., Springer US, Boston, MA, 285–308, https://doi.org/10.1007/978-1-4613-2805-6_12, 1984.

Sarro, F., Moussa, R., Petrozziello, A., and Harman, M.: Learning From Mistakes: Machine Learning Enhanced Human Expert Effort Estimates, IEEE Trans. Softw. Eng., 48, 1868–1882, https://doi.org/10.1109/TSE.2020.3040793, 2022.

Scott, D., Hall, C. M., Rushton, B., and Gössling, S.: A review of the IPCC Sixth Assessment and implications for tourism development and sectoral climate action, J. Sustain. Tour., 0, 1–18, https://doi.org/10.1080/09669582.2023.2195597, 2023.

Seemuangngam, A. and Lin, H.-L.: The impact of urbanization on urban flood risk of Nakhon Ratchasima, Thailand, Appl. Geogr., 162, 103152, https://doi.org/10.1016/j.apgeog.2023.103152, 2024.

Shafizadeh-Moghadam, H., Valavi, R., Shahabi, H., Chapi, K., and Shirzadi, A.: Novel forecasting approaches using combination of machine learning and statistical models for flood susceptibility mapping, Journal of environmental management, 217, 1–11, 2018.

Sinha, R., Bapalu, G. V., Singh, L. K., and Rath, B.: Flood risk analysis in the Kosi river basin, north Bihar using multi-parametric approach of Analytical Hierarchy Process (AHP), J. Indian Soc. Remote Sens., 36, 335–349, https://doi.org/10.1007/s12524-008-0034-y, 2008.

Sun, B., Fang, C., Liao, X., Guo, X., and Liu, Z.: The relationship between urbanization and air pollution affected by intercity factor mobility: A case of the Yangtze River Delta region, Environ. Impact Assess. Rev., 100, 107092, https://doi.org/10.1016/j.eiar.2023.107092, 2023.

Tang, Z., Wang, P., Li, Y., Sheng, Y., Wang, B., Popovych, N., and Hu, T.: Contributions of climate change and urbanization to urban flood hazard changes in China’s 293 major cities since 1980, J. Environ. Manage., 353, 120113, https://doi.org/10.1016/j.jenvman.2024.120113, 2024.

Vincent, A. M., K.s.s., P., and Jidesh, P.: Flood susceptibility mapping using AutoML and a deep learning framework with evolutionary algorithms for hyperparameter optimization, Appl. Soft Comput., 148, 110846, https://doi.org/10.1016/j.asoc.2023.110846, 2023.

Wagenaar, D., Curran, A., Balbi, M., Bhardwaj, A., Soden, R., Hartato, E., Mestav Sarica, G., Ruangpan, L., Molinario, G., and Lallemant, D.: Invited perspectives: How machine learning will change flood risk and impact assessment, Nat. Hazard. Earth Sys., 20, 1149–1161, https://doi.org/10.5194/nhess-20-1149-2020, 2020.

Wan, H., Zhong, Z., Yang, X., and Li, X.: Impact of city belt in Yangtze River Delta in China on a precipitation process in summer: A case study, Atmos. Res., 125–126, 63–75, https://doi.org/10.1016/j.atmosres.2013.02.004, 2013.

Wang, M., ~~Li, Y., Yuan, H., Zhou, S., Wang, Y., Adnan Ikram, R. M., and Li, J.: An XGBoost-SHAP approach to quantifying morphological impact on urban flooding susceptibility, Ecol. Indic., 156, 111137, https://doi.org/10.1016/j.ecolind.2023.111137, 2023a.~~

~~Wang, M.,~~ Fu, X., Zhang, D., Chen, F., Liu, M., Zhou, S., Su, J., and Tan, S. K.: Assessing urban flooding risk in response to climate change and urbanization based on shared socio-economic pathways, Science of The Total Environment, 880, 163470, https://doi.org/10.1016/j.scitotenv.2023.163470, ~~2023b~~2023a.

Wang, P., Li, Y., Yu, P., and Zhang, Y.: The analysis of urban flood risk propagation based on the modified susceptible infected recovered model, J. Hydrol., 603, 127121, https://doi.org/10.1016/j.jhydrol.2021.127121, 2021.

Wang, T., Wang, H., Wang, Z., and Huang, J.: Dynamic risk assessment of urban flood disasters based on functional area division—A case study in Shenzhen, China, J. Environ. Manage., 345, 118787, https://doi.org/10.1016/j.jenvman.2023.118787, ~~2023c~~2023b.

Wang, Y., Liu, G., Guo, E., and Yun, X.: Quantitative Agricultural Flood Risk Assessment Using Vulnerability Surface and Copula Functions, Water, 10, 1229, https://doi.org/10.3390/w10091229, 2018.

Xu, H., Hou, X., Pan, S., Bray, M., and Wang, C.: Socioeconomic impacts from coastal flooding in the 21st century China's coastal zone: A coupling analysis between coastal flood risk and socioeconomic development, Sci. Total Environ., 917, 170187, 2024.

Yan, M., Yang, J., Ni, X., Liu, K., Wang, Y., and Xu, F.: Urban waterlogging susceptibility assessment based on hybrid ensemble machine learning models: A case study in the metropolitan area in Beijing, China, J. Hydrol., 630, 130695, 2024.

Yang, W., Xu, K., Lian, J., Ma, C., and Bin, L.: Integrated flood vulnerability assessment approach based on TOPSIS and Shannon entropy methods, Ecol. Indic., 89, 269–280, https://doi.org/10.1016/j.ecolind.2018.02.015, 2018.

Yang, X., Li, H., Zhang, J., Niu, S., and Miao, M.: Urban economic resilience within the Yangtze River Delta urban agglomeration: Exploring spatially correlated network and spatial heterogeneity, Sustainable Cities and Society, 103, 105270, https://doi.org/10.1016/j.scs.2024.105270, 2024.

Yuan, X., Chen, C., Lei, X., Yuan, Y., and Muhammad Adnan, R.: Monthly runoff forecasting based on LSTM–ALO model, Stoch. Env. Res. Risk A., 32, 2199–2212, https://doi.org/10.1007/s00477-018-1560-y, 2018.